SURE 静岡大学学術リポジトリ
Shizuoka University REpository

Design of potent ABA receptor antagonists based on a conformational restriction approach

メタデータ	言語: English 出版者: 公開日: 2020-07-28 キーワード (Ja): キーワード (En): 作成者: Takeuchi, Jun, Nagamiya, Hikaru, Moroi, Sayaka, Ohnishi, Toshiyuki, Todoroki, Yasushi メールアドレス: 所属:
URL	http://hdl.handle.net/10297/00027562

Design of potent ABA receptor antagonists based on a conformational restriction approach

Jun Takeuchi[1]*, Hikaru Nagamiya[1], Sayaka Moroi[1], Toshiyuki Ohnishi[1,2] & Yasushi Todoroki[1,2]*

[1]*Faculty of Agriculture, Shizuoka University, Shizuoka 422-8529, Japan*

[2]*Research Institute of Green Science and Technology, Shizuoka University, Shizuoka 422-8529, Japan.*

Corresponding Authors

*E-mail: takeuchi.jun@shizuoka.ac.jp

*E-mail: todoroki.yasushi@shizuoka.ac.jp

†Electronic supplementary information (ESI) available: Supplementary figures and NMR spectra of synthesized compounds. See DOI:

Abstract

The physiological functions of the plant hormone abscisic acid (ABA) are triggered by interactions between PYR/PYL/RCAR receptors (PYLs) and group-A protein phosphatases 2C (PP2Cs). PYL agonists/antagonists capable of inducing/disrupting these interactions would be valuable in investigating the regulatory mechanisms of ABA signaling. Previously, we developed (+)-PAO4, a high-affinity PYL antagonist, by conformationally restricting the *S*-hexyl chain of our first reported PYL antagonist, 3′-hexylsulfanyl-ABA. Although (+)-PAO4 shows a greater binding affinity for *Arabidopsis* PYL5 compared with 3′-hexylsulfanyl-ABA, it is not able to completely block the ABA responses both *in vitro* and *in vivo*. Therefore, we designed novel conformationally restricted PYL antagonists in which the *O*-butyl chain of (+)-PAO4 was replaced with a pentyl (PAC4), a pentyne (PAT3) or a pentadiyne (PATT1) chain. (+)-PAT3 and (+)-PATT1 suppressed the ABA-induced inhibition of *Arabidopsis* seed germination more strongly than (+)-PAO4, but contrary to expectations, the affinity of each compound for PYL5 was almost the same as that of (+)-PAO4. Subsequent biochemical analyses revealed that unlike (+)-PAO4, (+)-PAT3 and (+)-PATT1 completely abolished ABA-induced PYL–PP2C interactions without partial agonistic activities. The superior PYL antagonist functions of (+)-PAT3 and (+)-PATT1 over (+)-PAO4 may explain their potent antagonistic activities against exogenous ABA *in vivo*. Furthermore, (+)-PAT3 and (+)-PATT1 also suppressed ABA responses in rice, indicating that both compounds are useful chemical tools for ABA-signaling studies, not only in dicots but also in monocots.

Introduction

Plants are sessile and unable to avoid environmental stresses, such as drought, high temperature and high salinity, which often limit plant productivity[1–3]. The plant hormone abscisic acid (ABA) is essential for coping with environmental changes and plays crucial roles in many physiological processes, such as seed dormancy and stomatal closure[4]. To date, core ABA-signaling components have been established in many plant species. Upon drought stress, ABA accumulates and binds to its receptors PYR/PYL/RCAR (PYR1 and PYLs 1–13 in *Arabidopsis*; hereafter referred to as PYLs), which subsequently inhibit group-A protein phosphatases 2C (PP2Cs)[5,6], resulting in the release of SNF1-related protein kinases (SnRK2s) from inhibition[7,8]. The full activation of SnRK2s requires phosphorylation by MAPKK-kinases and/or persulfurization by hydrogen sulfide[9,10], in addition to autophosphorylation after release from PP2C-mediated inhibition[11]. The activated SnRK2s phosphorylate transcription factors and S-type anion channels to elicit stress responses[12]. In unstressed plants, the target of rapamycin (TOR) kinase phosphorylates PYLs to prevent ABA actions[13].

PYLs represent the largest family of hormone receptors in plants. In addition to *Arabidopsis*, rice (*Oryza sativa*; 12)[14], maize (11)[15], tomato (15)[16], soybean (23)[17] and many other plants have more than 10 PYL orthologs, which contribute additively to the regulation of ABA responses in each plant. Because of this genetic redundancy, functional characterization of PYLs in plants using conventional molecular genetic approaches is daunting, although high-order *pyl* mutants in *Arabidopsis* and rice have been generated using a CRISPR/Cas9 gene editing system[18,19]. In this situation, a broad-spectrum PYL antagonist, a chemical compound capable of disrupting the functions of all PYLs, would be a powerful tool in circumventing the genetic redundancy[20]. Such a tool is particularly needed for ABA-signaling studies in plant systems lacking genetic resources. Therefore, we focused on the structural mechanism of a PYL–PP2C co-receptor system for ABA to develop PYL antagonists. By binding to PYLs,

ABA induces a conformational change in a mobile loop (gate), triggering its closure and enabling the receptor to inhibit PP2Cs. In PYL–ABA complexes, ABA is deeply embedded in the ligand-binding domain, leading to the formation of a tightly packed pocket of PYL residues; however, two small tunnels exist at ABA's 3′-CH (3′-tunnel) and 4′-C=O (4′-tunnel), and the entrances of these tunnels lie in the PP2Cs-binding interface. Based on this observation, we have reported three types of PYL antagonists to date; 3′-hexylsulfanyl-ABA (AS6)[21], propenyl-ABA with an *O*-butyl chain (PAO4)[22] and 4′-*O*-tolylpropynyl-ABA (PANMe)[23]. AS6 and (+)-PAO4 were developed by targeting the 3′-tunnel, and PANMe was designed to prevent the insertion of the Trp-indoles of PP2Cs into the 4′-tunnel. These PYL antagonists bind the ABA-binding pockets in PYLs and induce conformational changes to the gate-closed form in a manner similar to PYL–ABA complex formation, in which the substituents introduced into those compounds protruded through the tunnels and inhibited ABA-induced PYL–PP2C interactions by their direct steric hindrance. Therefore, all the compounds suppress ABA responses in *Arabidopsis*, although to varying degrees. Nevertheless, in monocots, such as rice, only (+)-PAO4 relieves the exogenous ABA-induced inhibition of seed germination (ESI Fig. S1). Although the reasons why AS6 and PANMe do not act as ABA antagonists in rice remain obscure, this result suggests that (+)-PAO4 is a suitable lead compound for developing ABA antagonists with broad-inhibitory spectra.

Despite the potential value of (+)-PAO4 to act as an effective ABA antagonist in both dicots and monocots, its potency is insufficient; (+)-PAO4 does not completely block ABA's actions both *in vitro* and *in vivo*. For instance, (+)-PAO4, unlike PANMe, does not completely inhibit ABA-induced PYL–PP2C interactions, probably because of its insufficient affinity for PYLs and/or its basal partial agonistic activity [(+)-PAO4 only weakly suppresses the activities of PP2Cs in a PYL-dependent manner]. Because of its incomplete activity as a PYL antagonist[22], (+)-PAO4 did not completely restore the germination time course of ABA-treated seeds to that

of the untreated seeds[23]. Therefore, in the present study, we modified the structure of (+)-PAO4 using a conformational restriction strategy, which has been widely used in drug design to create potent and/or selective ligands[24], to develop a more potent PYL antagonist. Because the (+)-PAO4 developed using this strategy bound more strongly to PYL5 than the lead compound AS6[22], we hypothesized that an increase in the rigidity of the ligand would increase the affinity for PYLs by reducing the entropic penalty of binding events. Here, we describe the design and preparation of conformationally restricted analogs of (+)-PAO4 and their PYL antagonistic activities both *in vitro* and *in vivo*. Of the three (+)-PAO4 analogs, (+)-PAT3 completely abolished ABA-induced PYL–PP2C interactions *in vivo* and almost restored the delayed germination time courses of ABA-treated seeds of *Arabidopsis* and rice to those of the respective untreated seeds without any adverse effects. Thus, (+)-PAT3 is a more effective PYL antagonist than (+)-PAO4 when used as a chemical tool for ABA-signaling studies.

Results and discussion

Design and synthesis

The tetralone skeleton and the long substituent at C-11′ of (+)-PAO4 are critical for PYL antagonistic activities in both *Arabidopsis* and rice. To function as a PYL antagonist, the substituent introduced into an ABA analog should be long enough to block PP2Cs binding and thin enough to fit into the 3′- or 4′-tunnel without interfering with the gate closures of PYLs. The *O*-butyl chain of (+)-PAO4 meets both requirements. The superposition of (+)-PAO4 and AS6 in the PYR1–AS6 complex (PDB ID: 3WG8) indicated that the *O*-butyl chain was accommodated in the 3′-tunnel[22]. Additionally, the affinity of (+)-PAO4 was 3-fold greater than that of AS6 with the more flexible *S*-hexyl chain owing to an entropic advantage. This suggested that further conformational restrictions of the *O*-butyl chain may increase the affinity for PYLs

by decreasing the entropy loss associated with complex formation. However, because the base (-O-CH_2-) of the *O*-butyl chain of (+)-PAO4 is located within the 3′-tunnel, the introduction of a large substituent such as benzene ring at this position may decrease the affinity for PYLs by inhibiting gate closure.

Taking into account the above considerations, we designed the following novel PYL antagonists: (+)-PAC4 (compound **2**), (+)-PAT3 (compound **3**) and (+)-PATT1 (compound **4**), in which the *O*-butyl chain of (+)-PAO4 was replaced with a pentyl, a pentyne and a pentadiyne chain, respectively, to reduce the conformational flexibility (Fig. 1). These (+)-PAO4 analogs were expected to be more potent PYL antagonists than (+)-PAO4 because of their higher affinities for the receptors. (±)-PAC4 was synthesized as shown in Scheme 1. Compound **5** was converted to triflate **6** using trifluoromethanesulfonic anhydride and 2,6-lutidine. The pentyl chain was introduced by Suzuki coupling of **6** with *n*-octyl-BBN to yield compound **7**[25]. The side chain was introduced by the direct addition of (*Z*)-3-methyl-2-penten-4-yn-1-ol using *n*-butyllithium, generating the alcohol **8**. Reduction (generating compound **9**), oxidation and esterification of **8** resulted in the formation of the ester **10**. Benzylic oxidation with pyridinium dichromate and *tert*-butyl hydroperoxide resulted in ketone, followed by the basic hydrolysis of the ester to give (±)-PAC4 (**2**). (±)-PAT3 was synthesized from commercially available 6-amino-1-tetralone. First, 6-amino-1-tetralone was treated with $NaNO_2$ in aqueous HCl, followed by the addition of KI to yield 6-iodo-1-tetralone **11**[26]. Dimethylation of compound **11** was achieved using methyl iodide in the presence of sodium hydride, followed by the introduction of the side chain, yielding compound **13** (Scheme 2). The pentyne chain was introduced by Sonogashira coupling, generating compound **14**. The reduction, oxidation and esterification of **14** resulted in the formation of the ester **16**. Benzylic oxidation, followed by the basic hydrolysis of the ester produced (±)-PAT3. (±)-PATT1 was synthesized from intermediate **13** as shown in Scheme 3. A trimethylsilylacetylene moiety was introduced by

Sonogashira coupling, yielding the trimethylsilyl-protected compound **17**. Reduction of the triple bond with SMEAH resulted in allylic alcohol, which was deprotected by potassium carbonate in MeOH to yield compound **18**. The oxidation and esterification of **18** resulted in the formation of the ester **19**, which was treated with *N*-bromosuccinimide and catalytic silver (I) nitrate to yield the bromoalkyne **20**. A terminal propyne was introduced by Cadiot–Chodkiewicz cross-coupling in the presence of $Pd(PPh_3)_2Cl_2$/CuI catalyst and diisopropylamine[27]. Benzylic oxidation, followed by the basic hydrolysis of the ester produced (±)-PATT1. All the (±)-PAO4 analogs were optically resolved using HPLC with a chiral column. These enantiomers were identified by the spectral data (ESI Fig. S2) using the circular dichroism (CD) exciton chirality method. Because the Cotton effects in the CD spectra of (+)- and (−)-PAC4/PAT3/PATT1 were similar to those of (1′*S*)-(+)- and (1′*R*)-(−)-PAO4[22], respectively, the absolute configuration at C-1′ was determined to be *S* for (+)-PAC4/PAT3/PATT1 and *R* for their (−)-isomers. In addition, similar to (−)-PAO4, (−)-PAC4, (−)-PAT3 and (−)-PATT1 showed no antagonistic activities (ESI Fig. S3), probably because they were not able to bind to PYLs owing to the steric hindrance of the pentyl, pentyne, and pentadiyne chains, respectively. This also supported the absolute configurations of PAC4, PAT3 and PATT1 as determined by the CD spectra.

Physiological effects of (+)-PAC4, (+)-PAT3 and (+)-PATT1 on *Arabidopsis* seed germination

The bioactivities of (+)-PAC4, (+)-PAT3 and (+)-PATT1 were examined using an *Arabidopsis* seed germination assay. In this assay, a PYL agonist inhibits seed germination, whereas a PYL antagonist relieves the inhibition of seed germination when coapplied with ABA. None of the (+)-PAO4 analogs inhibited seed germination, and they all suppressed the ABA-induced inhibition (Fig. 2). (+)-PAT3 and (+)-PATT1 showed stronger antagonistic activities than (+)-PAO4. At concentrations more than 3-fold that of ABA, both compounds almost restored the delayed germination time course of ABA-treated seeds relative to that of untreated seeds,

whereas (+)-PAO4 was unable to achieve the same effect at such concentrations. This property of (+)-PAT3 and (+)-PATT1 as antagonists was similar to that of PANMe, a potent and complete PYL antagonist we developed previously[23], and the antagonistic potency of (+)-PAT3 and (+)-PATT1 was comparable to that of PANMe (ESI Fig. S4). The physiological data suggested that (+)-PAT3 and (+)-PATT1 would have greater affinities for PYLs compared with that of (+)-PAO4 and/or function as complete PYL antagonists without partial agonistic activities *in vitro*.

During early seedling growth after germination, (+)-PATT1 weakly inhibited cotyledon greening when present at a high 30-μM concentration (ESI Fig. S5). Because this phenomenon was not observed with other (+)-PAO4 analogs, the greening inhibition by (+)-PATT1 may be attributed to the diyne structure of the introduced chain. Several polyacetylenic compounds show cytotoxic activities, such as anticancer and neurotoxic, as well as anti-fungal activities[28,29]. Considering that the chlorophyll content in (+)-PATT1-treated seedlings was reduced to 60.2% compared with that of mock-treated controls (ESI Fig. S6), (+)-PATT1 may have altered chlorophyll biosynthesis and/or metabolism. Thus, (+)-PAT3 should be used as a chemical tool for disrupting ABA signaling when a 30 μM or higher concentration is required. At a concentration lower than 30 μM, (+)-PATT1 may be a useful alternative option.

Comparison of the (+)-PAO4 analogs' binding affinities to *Arabidopsis* PYLs

To determine whether the potent ABA antagonistic activities of (+)-PAT3 and (+)-PATT1 are dependent on increased affinities for the PYL receptors, we conducted isothermal titration calorimetry experiments. *Arabidopsis* PYLs are classified into two distinct subclasses on the basis of their oligomeric state: PYR1 and PYL1–3 form dimers in solution, whereas PYL4–12 exist as monomers. A monomeric receptor (PYL5) was selected over dimeric receptors because it displays simple ligand associations and dissociations and lacks a dimer dissociation step. The apparent dissociation constants (K_d's) and the thermodynamic constants, the change of enthalpy

(ΔH), entropy ($-T\Delta S$) and free energy (ΔG), for PYL5-(+)–PAC4/PAT3/PATT1 interactions are listed in Table 1. The K_d values of (+)-PAC4, (+)-PAT3 and (+)-PATT1 were determined to be 68, 93 and 129 nM (ESI Fig. S7), respectively, indicating that the affinities of (+)-PAC4, (+)-PAT3 and (+)-PATT1 may be nearly equivalent to that of (+)-PAO4. When compared with (+)-PAO4, (+)-PAC4/PAT3/PATT1 binding was associated with larger positive ΔS. This may be attributed to the expanding hydrophobic interactions and desolvation effects of the C5 hydrophobic chains in addition to the reduction of the entropy loss associated with the formation of the complexes. However, for the enthalpy change, (+)-PAC4 ($\Delta H = -6.5$ kcal mol^{-1}), (+)-PAT3 ($\Delta H = -3.7$ kcal mol^{-1}) and (+)-PATT1 ($\Delta H = -5.6$ kcal mon^{-1}) exhibited smaller negative values than (+)-PAO4 ($\Delta H = -6.7$ kcal mol^{-1}). Consequently, all the (+)-PAO4 analogs showed almost the same ΔG values. The small negative ΔH values for (+)-PAT3 and (+)-PATT1 may result from the induced-fit during receptor binding being hindered by the rigid pentyne and pentadiyne chains, respectively. Thus, the conformational restriction of the *O*-butyl chain of (+)-PAO4 does not effectively intensify the binding affinity for PYLs, which indicates that the potent ABA antagonistic activities of (+)-PAT3 and (+)-PATT1 were caused by factors other than their affinities for PYLs.

Comparison of the effects of (+)-PAO4 analogs on PYL–PP2C interactions

The K_d values of (+)-PAO4 analogs did not support the explanation that the potent bioactivities of (+)-PAT3 and (+)-PATT1 *in vivo* resulted from increases in the affinities for PYLs. Therefore, we conducted PP2C phosphatase assays using HAB1 as the PP2C and PYR1 and PYL1–6, 8 and 9 as the PYLs to investigate the effects of (+)-PAO4 analogs on PYL–PP2C interactions. In these assays, receptor activation was monitored by PP2C activity inhibition, and effective agonists, such as ABA, exhibited near-complete PP2C activity inhibition at saturating concentrations, whereas partial agonists failed to completely inhibit PP2C activity[21]. (+)-PAC4 showed weak inhibitory activity against the PP2C in the dimeric PYLs similar to (+)-PAO4

(Fig. 3A), which suggested that (+)-PAC4 acted as a partial agonist. In contrast, (+)-PAT3 and (+)-PATT1 did not significantly inhibit the PP2C in the presence of any of the tested PYLs. Next, the antagonistic effects of these compounds were evaluated by examining their ability to reverse ABA-dependent PP2C inhibition. ABA strongly inhibited the PP2C activity at 5 μM, resulting in a residual PP2C activity of <20%. (+)-PAT3 and (+)-PATT1 antagonized the ABA-dependent inhibition of PP2C activity more strongly than (+)-PAO4 (Fig. 3B; Fig. 4A). For example, (+)-PAO4 only recovered the PP2C activity to approximately 40% even at 100 μM in the presence of PYL2, whereas (+)-PAT3 and (+)-PATT1 achieved recovery levels of 80%–90% under the same conditions (Fig. 4A). These results indicated that the ligand profile of (+)-PAT3 and (+)-PATT1 was similar to that of PANMe (Fig. 3A, B)[23].

The effects of (+)-PAT3 and (+)-PATT1 on the PYL–PP2C interaction were further characterized by an *in vitro* pulldown assay using PYL2 in combination with HAB1 (Fig. 4B, C). (+)-PAO4 weakly induced the interaction of PYL2 with HAB1 and did not completely abolish the PYL2–HAB1 interaction because of its partial agonistic activity. In contrast, (+)-PAT3 and (+)-PATT1 did not induce the PYL2–HAB1 interaction and almost completely blocked the ABA-induced inhibition of this interaction. Thus, (+)-PAT3 and (+)-PATT1, unlike (+)-PAO4 and (+)-PAC4, functioned as complete PYL antagonists without partial agonistic activities in the *in vitro* assay system. This difference may explain the stronger antagonistic activities of (+)-PAT3 and (+)-PATT1 compared with those of (+)-PAO4 and (+)-PAC4 in the *Arabidopsis* seed germination assay. Namely, the greater bioactivities of (+)-PAT3 and (+)-PATT1 may be caused by the loss of partial agonistic activities. Because the linear lengths of the *O*-butyl/pentyl chains of (+)-PAO4 and (+)-PAC4 (each 4.9 Å) result in their protrusion into the PP2C-interacting surfaces of PYLs, the partial agonistic activities of (+)-PAO4 and (+)-PAC4 may be attributed to the flexibility of their *O*-butyl and pentyl chains, respectively. In binding to PYLs, the tip of the *O*-butyl/pentyl chain protruding from the 3′-tunnel may have

bent to the surfaces of the PYLs, as is the case for the *S*-hexyl chain of AS6, which has a similar *in vitro* partial agonistic activity[21]. In contrast, the pentadiyne chain of (+)-PATT1 is predicted to protrude straight out from the tunnel consequently blocking PYL–PP2C interactions more effectively than the *O*-butyl/pentyl chain (Fig. 5)[30], although further structural characterizations of PYL-(+)–PATT1 complexes are necessary to confirm this hypothesis.

Effects of (+)-PAT3 and (+)-PATT1 on a monocot crop, rice

To date, several PYL antagonists have been developed, and their effects have been demonstrated predominantly in dicots, such as *Arabidopsis* and lettuce, while there have been few reports describing effective ABA antagonists against monocots. Therefore, we investigated the effects of (+)-PAT3 and (+)-PATT1 on a monocot crop, rice. In the *in vitro* PP2C assays using a rice PYL (OsPYL2), (+)-PAT3 and (+)-PATT1 did not inhibit PP2C (OsPP2C06) activity in the presence of OsPYL2 and recovered the ABA-induced OsPP2C06 inhibition more strongly than (+)-PAO4 (Fig. 6A), which was consistent with the results of the *Arabidopsis* PP2C assays. Next, we determined whether (+)-PAT3 and (+)-PATT1 antagonized ABA actions *in vivo*. Both compounds, similar to (+)-PAO4, relieved the exogenous ABA-induced inhibition of seed germination and seedling growth (Fig. 6B; ESI Fig. S8). Thus, the effects of (+)-PAT3 and (+)-PATT1 were not restricted to dicots, such as *Arabidopsis*.

Conclusions

In this study, we designed three novel PYL antagonists as conformationally restricted analogs of (+)-PAO4, a PYL antagonist we developed previously, to improve its affinity for PYLs by reducing the entropic penalty on binding to the receptors and intensifying its antagonistic activity in plants. Among those analogs, (+)-PAT3 and (+)-PATT1 showed stronger ABA antagonistic activities than (+)-PAO4. Unexpectedly, however, their affinities for PYL5 were

almost the same as that of (+)-PAO4. Biochemical analyses revealed that, unlike (+)-PAO4, (+)-PAT3 and (+)-PATT1 completely abolished ABA-induced PYL–PP2C interactions probably because of their loss of partial agonistic activities. This superiority of (+)-PAT3 and PATT1 over (+)-PAO4 as PYL antagonists may explain their potent antagonistic activities against exogenous ABA *in vivo*. Taken together, our conformational restriction strategy applied to (+)-PAO4 was not very effective in increasing the affinity for PYLs but was effective in developing a complete PYL antagonist. Although we did not design (+)-PAT3 and (+)-PATT1 to lose the partial agonistic activity *in vitro*, its elimination may be more effective than the enhancement of the affinity for PYLs in the development of a potent PYL antagonist.

(+)-PAT3 and (+)-PATT1 not only acted as complete PYL antagonists in *Arabidopsis*, but also inhibited the ABA responses in rice. In a previous study, we showed that the inhibitory profiles of PYL antagonists differ greatly among plant species. For instance, PANMe is a potent ABA antagonist in *Arabidopsis* but does not relieve ABA's actions in monocots, including rice[23]. However, PANMe acted as an antagonist for both *Arabidopsis* and rice PYL in our *in vitro* phosphatase assays. Thus, as we previously noted, it is necessary to investigate whether ABA responses in all plants are controlled only by the widely accepted core ABA-signaling components revealed in the model plant *Arabidopsis*. In this context, (+)-PAT3 and (+)-PATT1 will be useful chemical tools for ABA-signaling studies, not only in dicots but also in monocots. Because a high concentration of (+)-PATT1 reduced the chlorophyll contents in *Arabidopsis* seedlings, probably because of off-target effects, (+)-PAT3 should be used as the primary tool to disrupt ABA signaling, although (+)-PATT1 at a low concentration may be a useful alternative option.

Conflicts of interest

There are no conflicts to declare.

Acknowledgements

We thank M. Okamoto for providing plasmid vectors, encoding PYLs and HAB1, and Toray Industries Inc., Tokyo, Japan, for the gift of (+)-ABA. This work was supported in part by the Japan Society for the Promotion of Science KAKENHI (17K19226 to J.T.). We thank Lesley Benyon, PhD, from Edanz Group (www.edanzediting.com/ac) for editing a draft of this manuscript.

Notes and references

1 P. Hasegawa, R. Bressan, J. Zhu and H. Bohnert, *Annu. Rev. Plant Biol.*, 2000, **51**, 463–499.

2 B. Li, K. Gao, H. Ren and W. Tang, *J. Integr. Plant Biol.*, 2018, **60**, 757–779.

3 S. M. Assmann and T. Jegla, *Curr. Opin. Plant Biol.*, 2016, **33**, 157–167.

4 D. P. Zhang, *Abscisic acid: metabolism, transport and signaling*, Springer Netherlands, Dordrecht, 2014.

5 S. R. Cutler, P. L. Rodriguez, R. R. Finkelstein and S. R. Abrams, *Annu. Rev. Plant Biol.*, 2010, **61**, 651–679.

6 X.-F. Wang and D.-P. Zhang, ABA signal perception and ABA receptors, *in Abscisic acid: metabolism, transport and signaling*, ed. D.-P. Zhang, Springer Netherlands, Dordrecht, 2014, pp. 89–116.

7 Y. Ma, I. Szostkiewicz, A. Korte, D. Moes, Y. Yang, A. Christmann and E. Grill, *Science*, 2009, **324**, 1064–1069.

8 S.-Y. Park, P. Fung, N. Nishimura, D. R. Jensen, H. Fujii, Y. Zhao, S. Lumba, J. Santiago, A. Rodrigues, T.-F. F. Chow, S. E. Alfred, D. Bonetta, R. Finkelstein, N. J. Provart, D. Desveaux, P. L. Rodriguez, P. McCourt, J.-K. Zhu, J. I. Schroeder, B. F. Volkman and S. R. Cutler, *Science*, 2009, **324**, 1068–71.

9 Y. Takahashi, J. Zhang, P. K. Hsu, P. H. O. Ceciliato, L. Zhang, G. Dubeaux, S. Munemasa, C. Ge, Y. Zhao, F. Hauser and J. I. Schroeder, *Nat. Commun.*, 2020, **11**, 12, DOI:10.1038/s41467-019-13875-y.

10 S. Chen, H. Jia, X. Wang, C. Shi, X. Wang, P. Ma, J. Wang, M. Ren and J. Li, *Mol. Plant*, 2020, **6**, 1–13.

11 L.-M. Ng, F.-F. Soon, X. E. Zhou, G. M. West, A. Kovach, K. M. Suino-Powell, M. J. Chalmers, J. Li, E.-L. Yong, J.-K. Zhu, P. R. Griffin, K. Melcher and H. E. Xu, *Proc. Natl. Acad. Sci.*, 2011, **108**, 21259–21264.

12 J. J. Weiner, F. C. Peterson, B. F. Volkman and S. R. Cutler, *Curr. Opin. Plant Biol.*, 2010, **13**, 495–502.

13 P. Wang, Y. Zhao, Z. Li, C.-C. Hsu, X. Liu, L. Fu, Y.-J. Hou, Y. Du, S. Xie, C. Zhang, J. Gao, M. Cao, X. Huang, Y. Zhu, K. Tang, X. Wang, W. A. Tao, Y. Xiong and J.-K. Zhu, *Mol. Cell*, 2018, **69**, 100-112.e6.

14 Y. He, Q. Hao, W. Li, C. Yan, N. Yan and P. Yin, *PLoS One*, 2014, **9**, e95246.

15 W. Fan, M. Zhao, S. Li, X. Bai, J. Li, H. Meng and Z. Mu, *BMC Plant Biol.*, 2016, **16**, 99.

16 M. González-Guzmán, L. Rodríguez, L. Lorenzo-Orts, C. Pons, A. Sarrión-Perdigones, M. A. Fernández, M. Peirats-Llobet, J. Forment, M. Moreno-Alvero, S. R. Cutler, A. Albert, A. Granell and P. L. Rodríguez, *J. Exp. Bot.*, 2014, **65**, 4451–4464.

17 G. Bai, D.-H. Yang, Y. Zhao, S. Ha, F. Yang, J. Ma, X.-S. Gao, Z.-M. Wang and J.-K. Zhu, *Plant Mol. Biol.*, 2013, **83**, 651–664.

18 Y. Zhao, Z. Zhang, J. Gao, P. Wang, T. Hu, Z. Wang, Y. J. Hou, Y. Wan, W. Liu, S. Xie, T. Lu, L. Xue, Y. Liu, A. P. Macho, W. A. Tao, R. A. Bressan and J. K. Zhu, *Cell Rep.*, 2018, **23**, 3340-3351.e5.

19 C. Miao, L. Xiao, K. Hua, C. Zou, Y. Zhao, R. A. Bressan and J.-K. Zhu, *Proc. Natl. Acad. Sci.*, 2018, **115**, 6058–6063.

20 Y. Ye, L. Zhou, X. Liu, H. Liu, D. Li, M. Cao, H. Chen, L. Xu, J. Zhu and Y. Zhao, *Plant Physiol.*, 2017, **173**, 2356–2369.

21 J. Takeuchi, M. Okamoto, T. Akiyama, T. Muto, S. Yajima, M. Sue, M. Seo, Y. Kanno, T. Kamo, A. Endo, E. Nambara, N. Hirai, T. Ohnishi, S. R. Cutler and Y. Todoroki, *Nat. Chem. Biol.*, 2014, **10**, 477–82.

22 J. Takeuchi, T. Ohnishi, M. Okamoto and Y. Todoroki, *Org. Biomol. Chem.*, 2015, **13**, 4278–4288.

23 J. Takeuchi, N. Mimura, M. Okamoto, S. Yajima, M. Sue, T. Akiyama, K. Monda, K. Iba, T. Ohnishi and Y. Todoroki, *ACS Chem. Biol.*, 2018, **13**, 1313–1321.

24 Z. Fang, Y. Song, P. Zhan, Q. Zhang and X. Liu, *Future Med. Chem.*, 2014, **6**, 885–901.

25 B. Ma, K. M. Guckian, E. Y. S. Lin, W. C. Lee, D. Scott, G. Kumaravel, T. L. Macdonald, K. R. Lynch, C. Black, S. Chollate, K. Hahm, G. Hetu, P. Jin, Y. Luo, E. Rohde, A. Rossomando, R. Scannevin, J. Wang and C. Yang, *Bioorganic Med. Chem. Lett.*, 2010, **20**, 2264–2269.

26 M. B. Nielsen, A. Kadziola, S. L. Broman, M. Rosenberg, J. Daub and O. Kushnir, *European J. Org. Chem.*, 2015, **2015**, 4119–4130.

27 N. Gulia, B. Pigulski and S. Szafert, *Organometallics*, 2015, **34**, 673–682.

28 Y. Chen, S. Peng, Q. Luo, J. Zhang, Q. Guo, Y. Zhang and X. Chai, *Chem. Biodivers.*, 2015, **12**, 474–502.

29 R. Negri, *Fitoterapia*, 2015, **106**, 92–109.

30 E. F. Pettersen, T. D. Goddard, C. C. Huang, G. S. Couch, D. M. Greenblatt, E. C. Meng and T. E. Ferrin, *J. Comput. Chem.*, 2004, **25**, 1605–12.

Figure legends

Fig. 1 Structures of (+)-PAO4 and its analogs

Fig. 2 Effects of (+)-PAC4, (+)-PAT3 and (+)-PATT1 on *Arabidopsis* seed germination compared with those of (+)-PAO4. Seed germination rate in the presence of 1 μM ABA and 3 μM (+)-PAO4 analogs (n = 3, error bars represent SDs).

Fig. 3 Effects of (+)-PAC4, (+)-PAT3 and (+)-PATT1 on PP2C phosphatase assays compared with those of (+)-PAO4. (A) Chemical inhibition of HAB1 by various ABA receptors in the presence of 50 μM of each test compound. (B) Antagonistic effect of each test compound against various ABA receptors. Assays were performed in the presence of 5 μM ABA and 50 μM of each test compound. (A, B) The concentration of each PYL was set at a 2:1 molar ratio to HAB1. The HAB1 phosphatase activity was normalized to a control (DMSO-treated) value of 100% (n = 3, error bars represent SD) and is expressed as relative activity.

Fig. 4 Effects of (+)-PAT3 and (+)-PATT1 on the PYL–PP2C interactions compared with those of (+)-PAO4. (A) Antagonistic effect of each test compound on PYL2 and PYL5 in the PP2C phosphatase assays. Assays were performed in the presence of 5 μM ABA and various concentrations (0, 5, 10, 20, 50 and 100 μM) of (+)-PAT3, (+)-PATT1 and (+)-PAO4. The concentration of each PYL was set at a 2:1 molar ratio to HAB1. The HAB1 phosphatase activity was normalized to a control (DMSO-treated) value of 100% (n = 3, error bars represent SD) and is expressed as relative activity. (B) Pulldown assay performed using purified glutathione S-transferase (GST)-HAB1 and 6xHis-tagged PYL2 (50 and 10 μg, respectively). Signals = (−) for 0 μM; (+) for 25 μM and (++) for 250 μM. (C) Relative amount of GST-HAB1 interacting with 6xHis-tagged PYL2. The amount of GST-HAB1 and 6xHis-tagged PYL2 on the gel (B) was measured using Image J 1.52a software, and the relative pulldown GST-HAB1 was calculated by normalizing 6xHis-tagged PYL2.

Fig. 5 Hypothetical antagonistic model of (+)-PATT1. (A) Model of (+)-PATT1–bound PYR1 constructed based on the crystal structure of the PYR1–AS6 complex. (+)-PATT1 is superimposed on AS6 in the PYR1–AS6 complex (PDB ID: 3WG8), where pentadiyne chain of (+)-PATT1 protrudes straight out from the 3′-tunnel. (B) Superposition of the model (A) with PYR1–ABA–HAB1 complex (gray, representing HAB1 only). The pentadiyne chain collided with HAB1 Val394, which is well conserved among PP2Cs. The solvent-excluded surface (probe radius: 1.4 Å) prepared with Chimera software. AS6, pink sticks; (+)-PATT1, purple sticks.

Fig. 6 Effects of (+)-PAT3 and (+)-PATT1 on rice (*Oryza sativa*) compared with those of (+)-PAO4. (A) Agonistic (left) and antagonistic (right) effects of (+)-PAO4, (+)-PAT3 and (+)-PATT1 on the OsPYL2–OsPP2C06 interaction. (+)-PAO4 analogs were tested at 0, 5, 10, 20,

50 and 100 μM, while 1 μM ABA was used in the reactions. The OsPP2C06 activity of each reaction was normalized to a control (DMSO-treated) value of 100% and is expressed as relative activity. OsPYL2 and OsPP2C06 proteins were used at 300 pmol and 60 pmol, respectively (*n* = 3, error bars represent SDs). (B) Seed germination rate in the presence of 20 μM ABA and 30 μM (+)-PAO4, (+)-PAT3 or (+)-PATT1 (*n* = 3, error bars represent SDs).

Scheme 1 Synthesis of (±)-PAC4.

Scheme 2 Synthesis of (±)-PAT3.

Scheme 3 Synthesis of (±)-PATT1.

Table 1 Apparent (+)-PAC4, (+)-PAO4 and (+)-PATT1 binding affinities for PYL5

Table of contents entry

Conformationally restricted analogs of (+)-PAO4, an abscisic acid receptor antagonist, were synthesized to improve its potency.

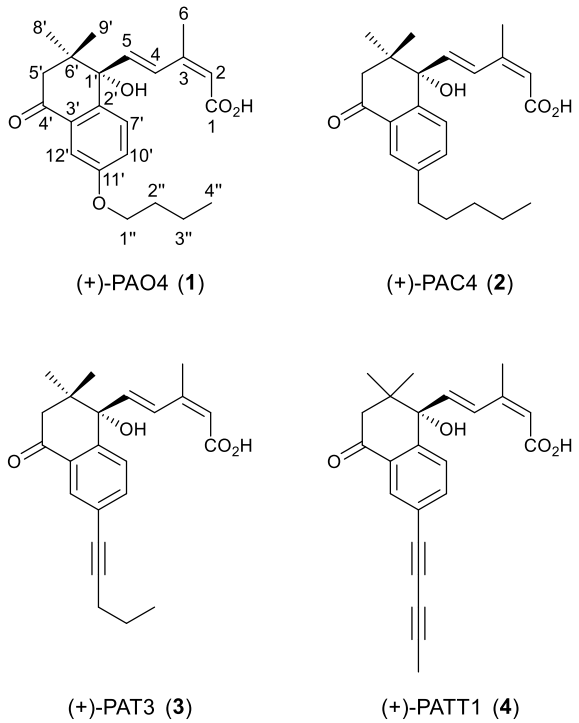

Fig. 1 Structures of (+)-PAO4 and its analogs.

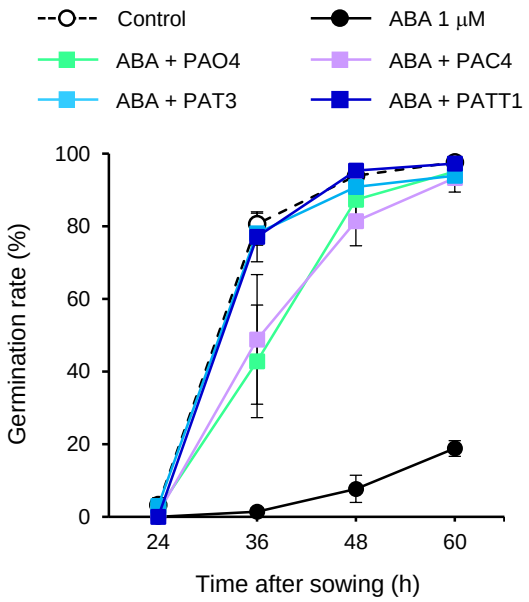

Fig. 2 Effects of (+)-PAC4, (+)-PAT3 and (+)-PATT1 on *Arabidopsis* seed germination compared with those of (+)-PAO4. Seed germination rate in the presence of 1 μM ABA and 3 μM (+)-PAO4 analogs (n = 3, error bars represent SDs).

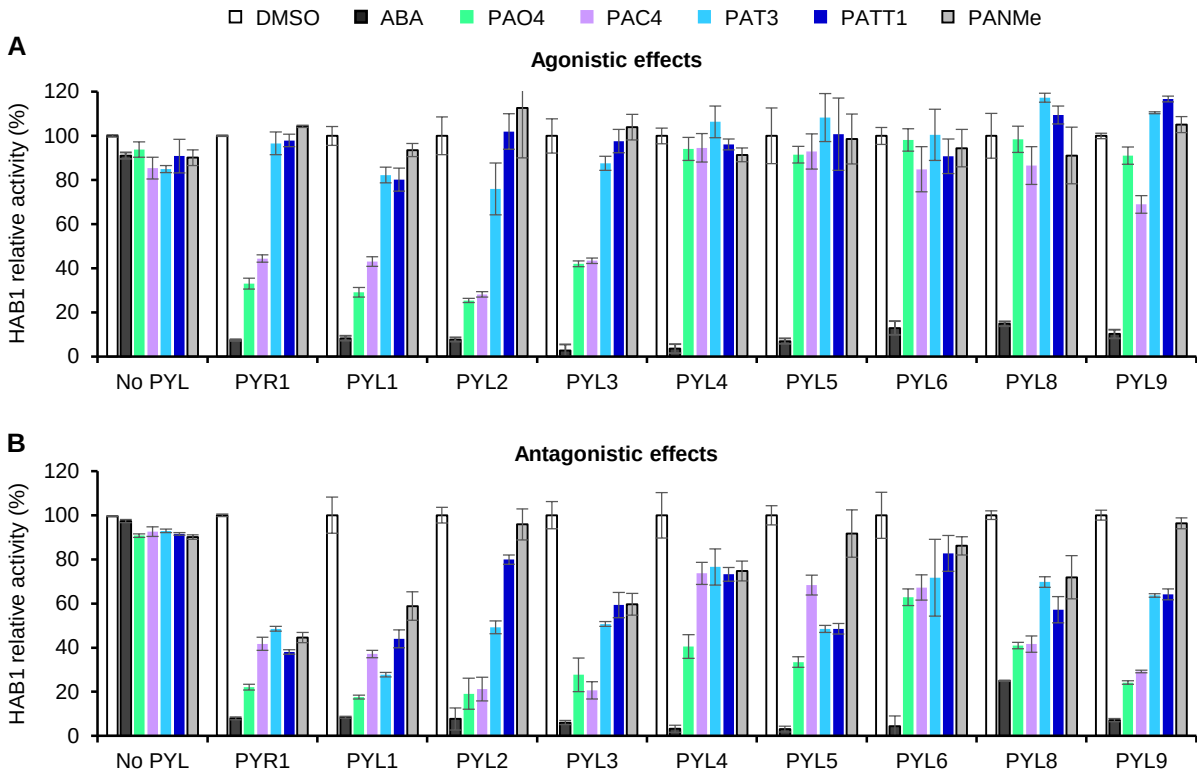

Fig. 3 Effects of (+)-PAC4, (+)-PAT3 and (+)-PATT1 on PP2C phosphatase assays compared with those of (+)-PAO4. (A) Chemical inhibition of HAB1 by various ABA receptors in the presence of 50 µM of each test compound. (B) Antagonistic effect of each test compound against various ABA receptors. Assays were performed in the presence of 5 µM ABA and 50 µM of each test compound. (A, B) The concentration of each PYL was set at a 2:1 molar ratio to HAB1. The HAB1 phosphatase activity was normalized to a control (DMSO-treated) value of 100% (n = 3, error bars represent SDs) and is expressed as relative activity.

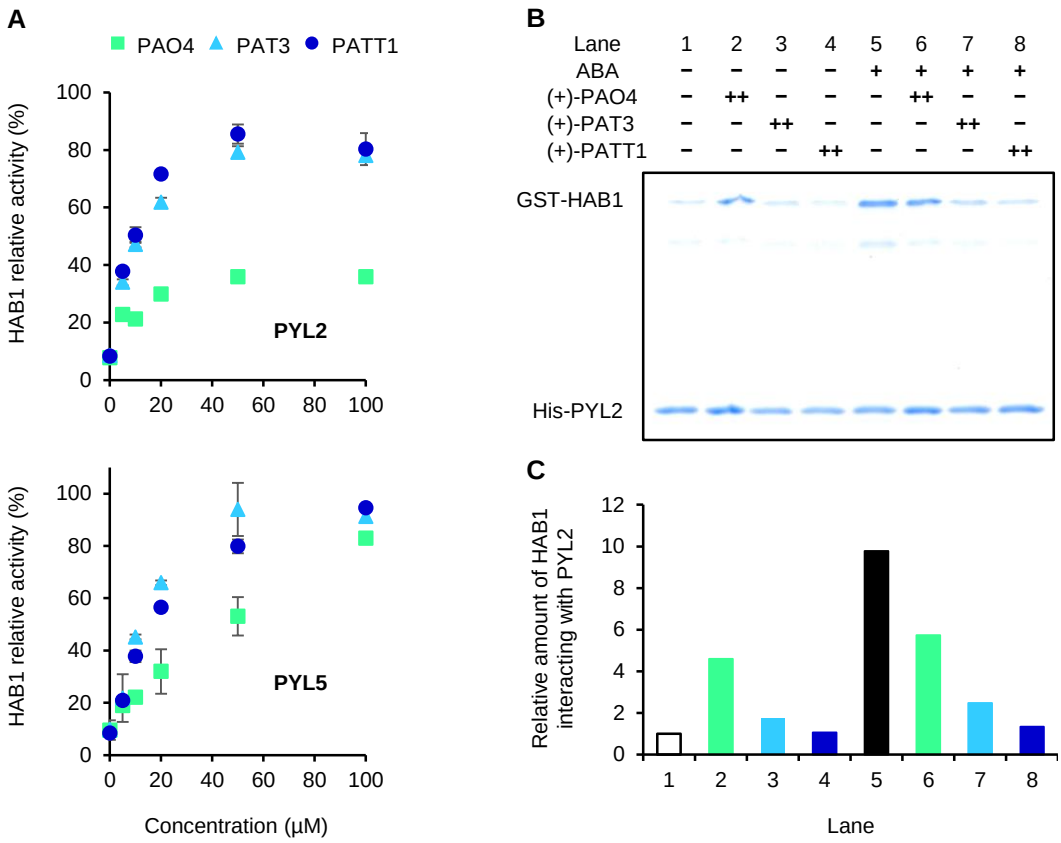

Fig. 4 Effects of (+)-PAT3 and (+)-PATT1 on the PYL–PP2C interactions compared with those of (+)-PAO4. (A) Antagonistic effect of each test compound on PYL2 and PYL5 in the PP2C phosphatase assays. Assays were performed in the presence of 5 μM ABA and various concentrations (0, 5, 10, 20, 50 and 100 μM) of (+)-PAT3, (+)-PATT1 and (+)-PAO4. The concentration of each PYL was set at a 2:1 molar ratio to HAB1. The HAB1 phosphatase activity was normalized to a control (DMSO-treated) value of 100% (n = 3, error bars represent SDs) and is expressed as relative activity. (B) Pulldown assay performed using purified glutathione S-transferase (GST)-HAB1 and 6xHis-tagged PYL2 (50 and 10 μg, respectively). Signals = (−) for 0 μM; (+) for 25 μM and (++) for 250 μM. (C) Relative amount of GST-HAB1 interacting with 6xHis-tagged PYL2. The amount of GST-HAB1 and 6xHis-tagged PYL2 on the gel (B) was measured using Image J 1.52a software, and the relative pulldown GST-HAB1 was calculated by normalizing 6xHis-tagged PYL2.

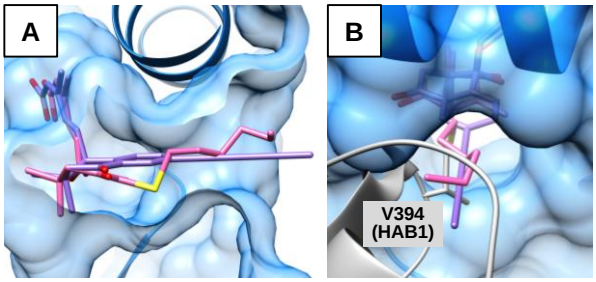

Fig. 5 Hypothetical antagonistic model of (+)-PATT1. (A) Model of (+)-PATT1-bound PYR1 constructed based on the crystal structure of the PYR1-AS6 complex. (+)-PATT1 is superimposed on AS6 in the PYR1-AS6 complex (PDB ID: 3WG8), where pentadiyne chain of (+)-PATT1 protrudes straight out from the 3′-tunnel. (B) Superposition of the model (A) with PYR1–ABA–HAB1 complex (gray, representing HAB1 only). The pentadiyne chain collided with HAB1 Val394, which is well conserved among PP2Cs. The solvent-excluded surface (probe radius: 1.4 Å) prepared with Chimera software. AS6, pink sticks; (+)-PATT1, purple sticks.

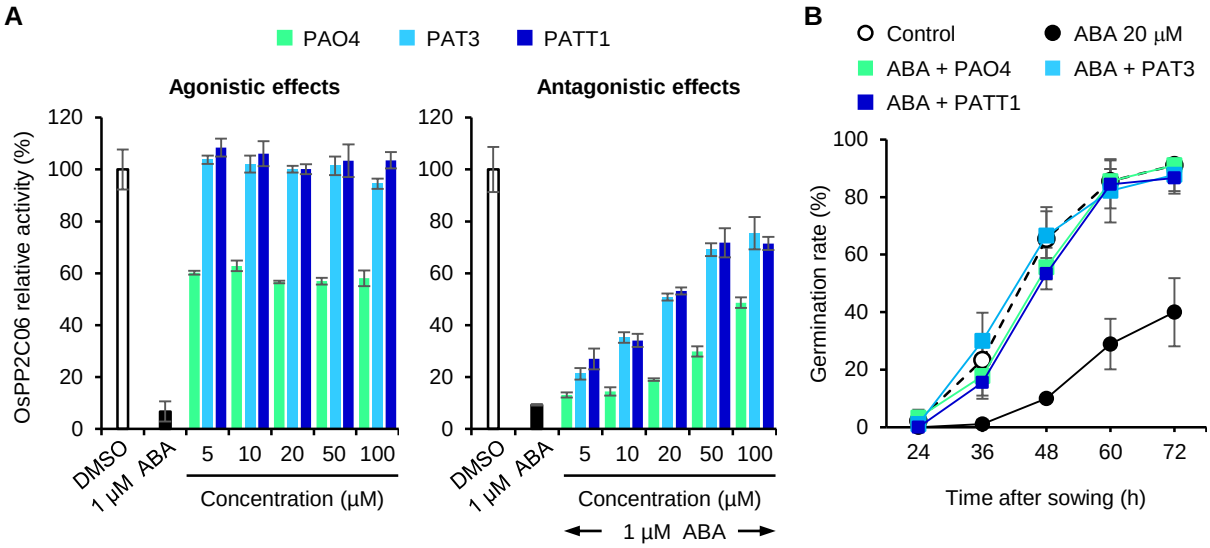

Fig. 6 Effects of (+)-PAT3 and (+)-PATT1 on rice (*Oryza sativa*) compared with those of (+)-PAO4. (A) Agonistic (left) and antagonistic (right) effects of (+)-PAO4, (+)-PAT3 and (+)-PATT1 on the OsPYL2–OsPP2C06 interaction. (+)-PAO4 analogs were tested at 0, 5, 10, 20, 50 and 100 μM, while 1 μM ABA was used in the reactions. The OsPP2C06 activity of each reaction was normalized to a control (DMSO-treated) value of 100% and is expressed as relative activity. OsPYL2 and OsPP2C06 proteins were used at 300 pmol and 60 pmol, respectively (n = 3, error bars represent SDs). (B) Seed germination rate in the presence of 20 μM ABA and 30 μM (+)-PAO4, (+)-PAT3 or (+)-PATT1 (n = 3, error bars represent SDs).

Table 1 Apparent (+)-PAC4, (+)-PAO4 and (+)-PATT1 binding affinities for PYL5

Compounds	K_d [a](nM)	ΔH (kcal/mol)	$-T\Delta S$[b] (kcal/mol)	ΔG[c] (kcal/mol)
(+)-PAC4	68 ± 18	−6.5 ± 0.1	−3.1	−9.6 ± 0.1
(+)-PAT3	93 ± 37	−3.7 ± 0.1	−5.7	−9.4 ± 0.2
(+)-PATT1	129 ± 33	−5.6 ± 0.1	−3.7	−9.2 ± 0.1
(+)-PAO4[d]	127 ± 38	−6.7 ± 0.1	−2.5	−9.2 ± 0.2

[a] K_d, ΔH obtained from single-set-of-sites fit to date.
[b] $T\Delta S = \Delta H - \Delta G$
[c] $\Delta G = -RTln(1/K_d)$. Uncertinties for K_d, ΔH, and ΔG calculated by curve fitting program of MicroCal Origin 7.0.
[d] Takeuchi *et al*., 2015

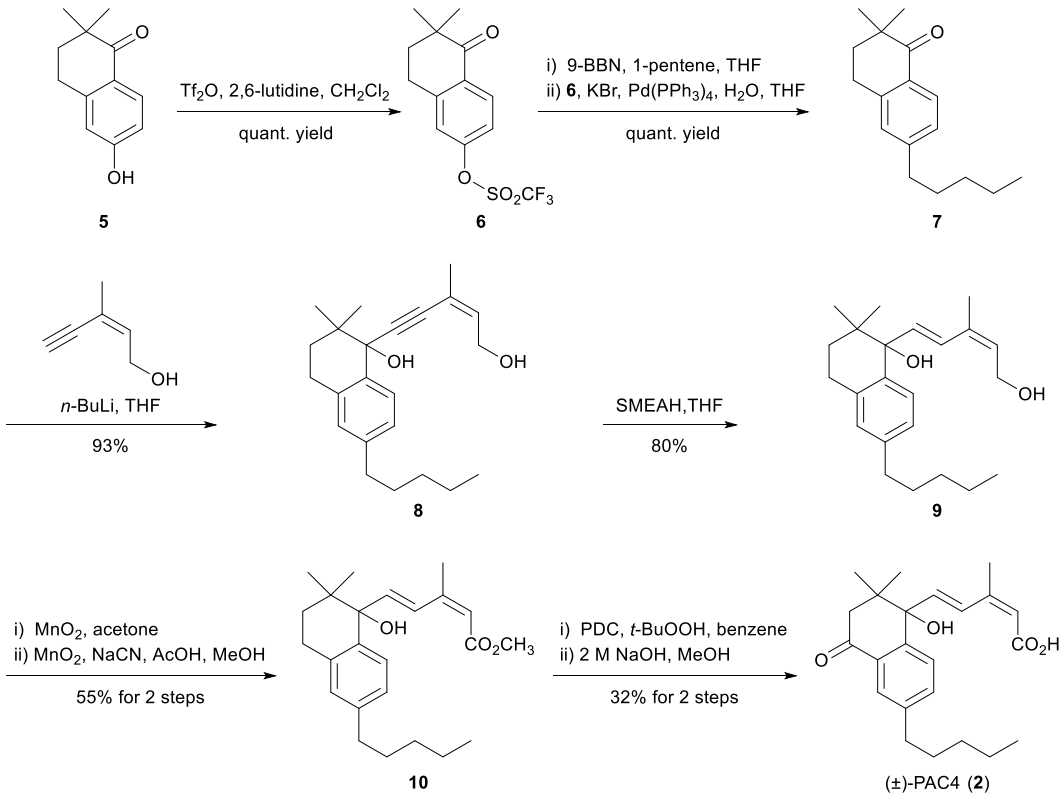

Scheme 1 Synthesis of (±)-PAC4.

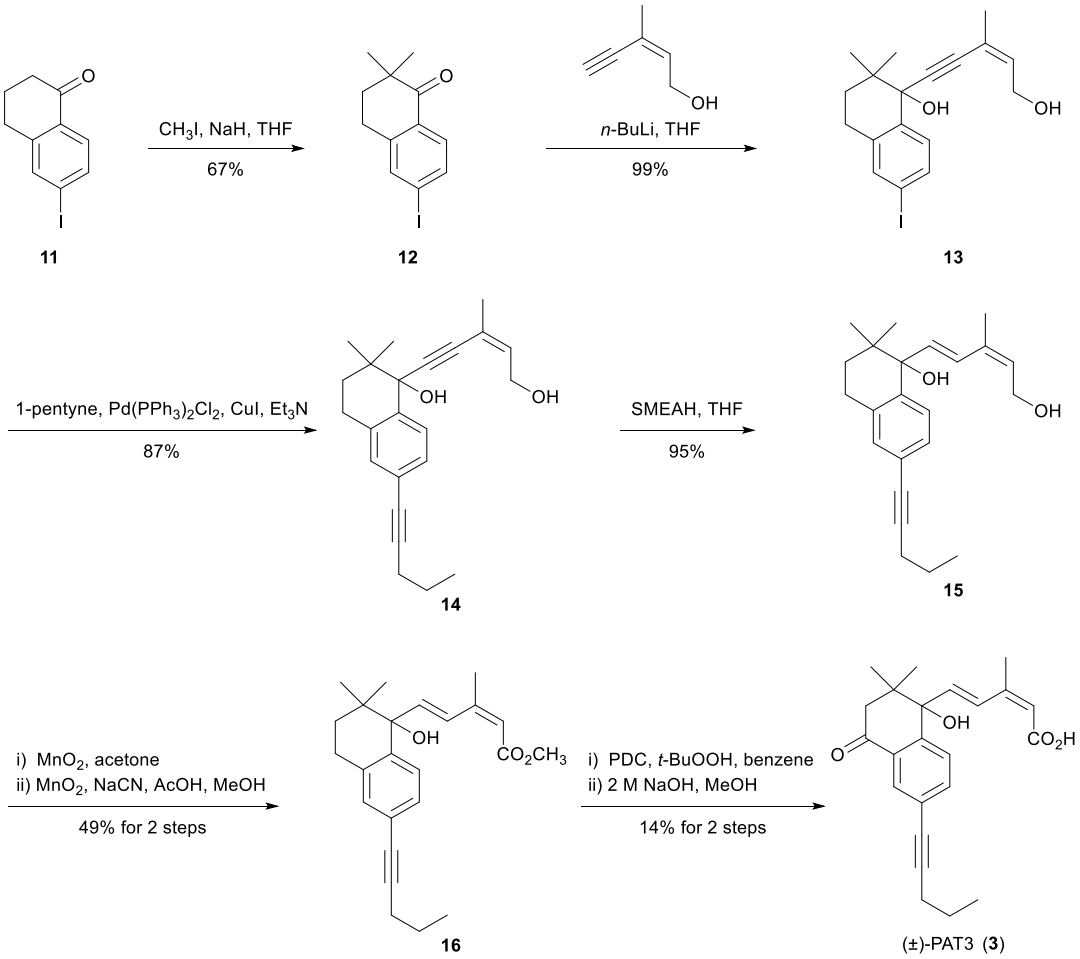

Scheme 2 Synthesis of (±)-PAT3.

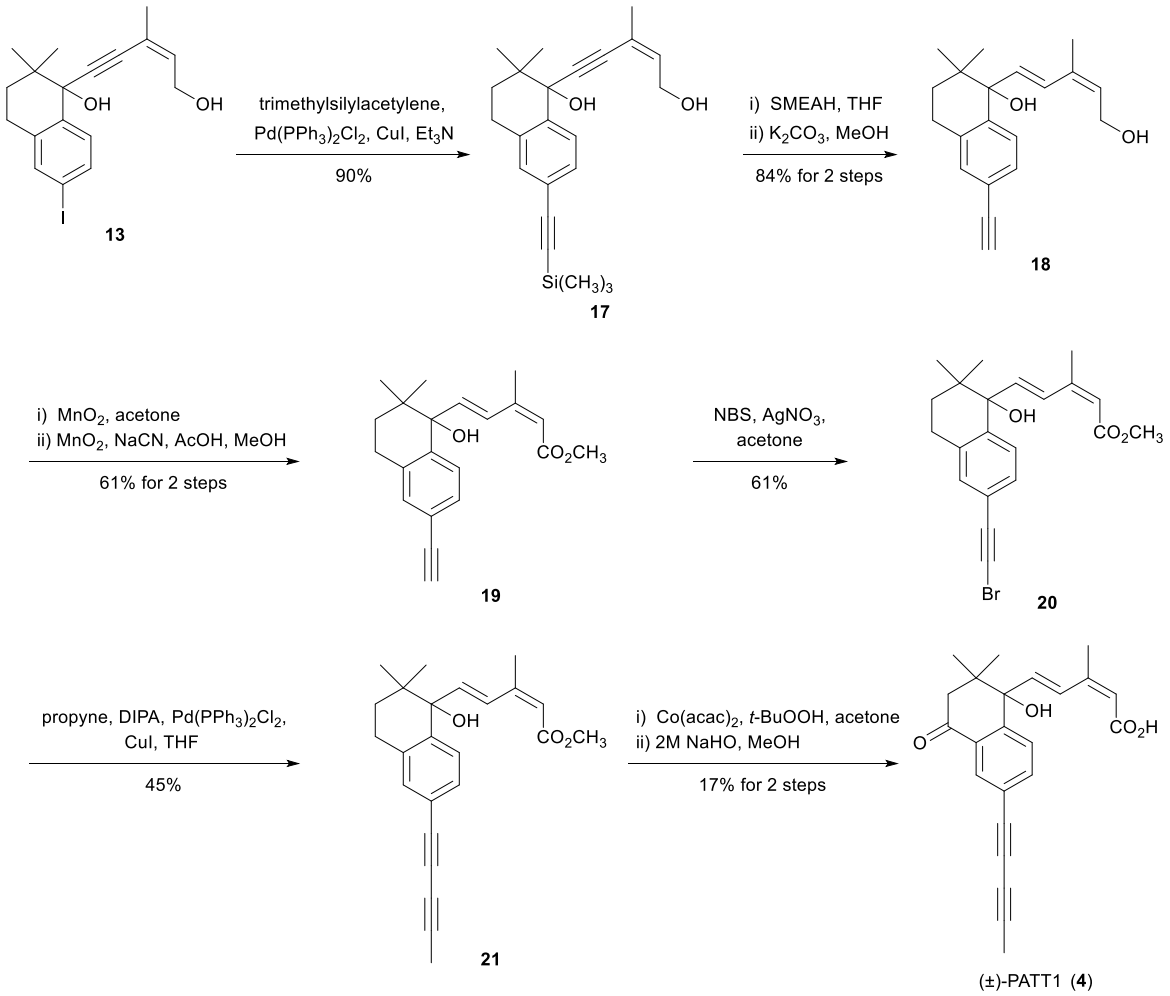

Scheme 3 Synthesis of (±)-PATT1.